Stiffness of Confinement Controls the Localization of an Object under Crowding: Macroscale Real-World and Microscale Numerical Modelings on the Specificity of Intracellular Positioning

Maho Kuroda[1*], Satoshi Takatori[1†] , Takahiro Kenmotsu[1‡] ,
Kenichi Yoshikawa[1,2§] , and Chwen-Yang Shew[3¶]

[1]*Faculty of Life and Medical Sciences, Doshisha University, Kyoto 610-0321, Japan*
[2]*Center for Integrative Medicine and Physics, Institute for Advanced Study, Kyoto University, Kyoto 606-8501, Japan*
[3]*Department of Chemistry, College of Staten Island, City University of New York, Staten Island, NY 10314, U.S.A.*

Macroscopic systems that mimic microscopic systems can provide fundamental understanding of how macromolecules (e.g., cellular organelles) are organized in a confined space. We studied the behavior of a large particle interacting with several small particles confined in dishes with hard/soft boundary conditions under mechanical vibration using a cm-scale model. We also performed a numerical simulation for the micro-scale system under Brownian fluctuation with fluctuation–dissipation, as a simple model of living cellular cytoplasmic crowding. Under a hard boundary condition, the large sphere preferred the boundary at low crowding but tended to localize to the interior under high crowding. Conversely, when the boundary was soft, the large sphere localized to the interior under low crowding and tended to migrate near the boundary when crowding increased. Interestingly, numerical modeling reproduced similar results for both the experimental hard and soft boundary conditions. Our models revealed that membrane stiffness can affect the organization of biopolymers within a confined space and may help explain cellular dynamics.

1. Introduction

Living cells self-organize their steric structure by adopting a highly crowded aqueous solution containing 30–40 weight % of macromolecules, such as DNA, RNA, and proteins.[1–4] In general, the cytoskeletal network is thought to play an important role in controlling the positions of various cellular organelles such as the nucleus, mitochondria, membrane-less organelles, etc. However, recent studies have suggested that crowding of biomolecules within the cytoplasmic solution plays an essential role in the formation and stability of subcellular organelles and the 3D structure of living cells.

The introduction of polymers at relatively high concentrations causes an attractive interaction between colloidal particles, based on stability studies of colloidal solutions. This experimental trend has been interpreted in terms of a depletion effect,[5–9] when normally self-avoiding large colloidal particles compact closer to each other in the presence of smaller particles (e.g., proteins). These smaller particles act as an entropic depletion force and can overcome the steric containment due to a self-avoiding effect of large colloidal particles the steric containment due to a self-avoiding effect of large colloidal particles is overcome by an attractive interaction among large particles through an entropic depletion force in the presence of smaller particles like proteins. Depletion interactions on colloidal particles should induce these particles to attach to a planar surface and to the boundary of confinement in a solution crowded with soluble polymers. According to this theoretical hypothesis of a depletion interaction,[10–13] organelles should be attracted to each other in crowded cellular fluids and attach to the inner membrane surface. On the contrary, organelles observed in living cells localized to the interior and avoided contact with the membrane surface, which is opposite to the situation predicted by the depletion theory. Thus, a phenomenological explanation of these seemingly repulsive interactions be-

tween organelles and the inner cellular-membrane surface must be examined by their physico-chemical parameters under biological conditions, such as their electronic charge.

Our work focuses on the importance of the boundary for the preferential positioning of confined macromolecules under crowding. Studies on the behavior of particles/objects under confinement have been actively carried out using both theoretical modeling[14–25] and experimental observations.[19,26–35] The theoretical work by Awazu showed segregation patterns of strongly and weakly fluctuating Brownian particles confined in a three-dimensional spherical container, under the assumptions that 1) a certain soft repulsion exists between the container wall and all particles and 2) that a certain short-range attraction exists between the wall and low mobility particles. When the container radius was sufficiently large, strongly or weakly fluctuating particles distributed near the periphery or the center of the container, respectively. In contrast, the distribution of fluctuating particles was inversed when the container was small.[23] Depending on the attraction strength between model chromatin and the nuclear membrane, chromatin distributed near the peripheral or inner regions during the dynamical nucleus deformation, a crucial mechanism for inverted chromatin positioning.[24] Cook et al. studied the behavior of two different kinds of polymers under confinement with a hard boundary condition by adapting the Monte Carlo simulation, identifying that entropic interactions among the polymers were essential to determine their positioning and conformation, which accounted for the specific changes observed in interface chromosomes.[25] In addition to the above-mentioned studies,[24,25] several simulation works have previously addressed the distribution of heterogeneous chromatin in a model nucleus (e.g., why certain genes are preferentially positioned in the peripheral or inner region of a nucleus). Most importantly, these studies provided preliminary insights into cellular morphology during apoptosis or necrosis.[36–38] However, fixed boundary conditions were used

to interpret the interactions between the wall of confinement and the entrapped substances in these previous studies.

We have recently quantitated the positioning of a large sphere in the presence of numerous small crowding spheres within confined cavities to gain insight into the mechanism that underlies self-organization in living cells. Our results showed that the position of a large spherical particle switched between the boundary and interior of a confined space depending on the parameters used, such as the number of small spheres and the interaction potential profile between the large sphere and smaller crowding spheres. We also observed a similar switching phenomenon for a simple real-world model of the position of a large sphere together with smaller crowding spheres.[13] Despite the progress made in the previous work, less attention has been focused on the effect of the structural boundaries for confined fluids. In biological systems, cellular membranes serve as boundaries to confine cellular materials. The stiffness of these membranes is significantly correlated with their cellular bioactivities.[39] Moreover, all eukaryotic cells in animals or plants contain membranes that separate intracellular components from the extracellular region. During cell death, large organelles are depleted, moving from the cytoplasm to the outside of the cell. For programmed cell death (i.e., apoptosis), cytoskeletons composed of actin filaments and protein tubulins degrade and rearrange in a way that causes the cell to shrink and break the cellular membrane into smaller blebs that surround and protect depleted organelles. For non-programmed cell death (i.e., necrosis), the weakened cell membrane swells and erupts. In either case, the rigidity of the cell boundary is reduced, and this enables the transport of cellular components across the membrane.[36–38] Inspired by these crucial cellular processes, we have devised a mechanical system using granular particles, which allows us to capture the essence of any morphologic changes of a confined system while the boundary rigidity is softened. In addition, the rigidity of the cellular membrane is associated with cancer cell migration and invasion.[40] These studies have clearly illustrated the importance of cellular membranes for their cell functions. The results of a recent vibration experiment by Downs and co-workers found that a quasi two-dimensional (2D) liquid/crystal transition can be either continuous or discontinuous depending on the elasticity of the boundary.[41] Despite the quasi 2D nature of the experiment, their work gives some insight into how the boundary may affect confined fluids contained within.[42]

Our present work is an extension of these studies. We have observed the position of a large particle surrounded by numerous smaller particles on a visible macroscopic scale under different boundary conditions. To mimic the effect of thermal fluctuations with a quasi 2D Brownian-like motion, we applied vibrational perturbation for the assembly of visible-sized particles using a vibrating plate. Previous experimental (real-world) models used granular objects under mechanical agitation and provided useful insight into the intrinsic behavior of how micro-objects assemble under thermal agitation, i.e., Brownian fluctuation.[13,43–50] Here we report that the position of a relatively large particle transitions between the inner and boundary regions when using a vibrational plate on a macroscopic crowding system with hard or soft boundaries. After discovering the specific effect
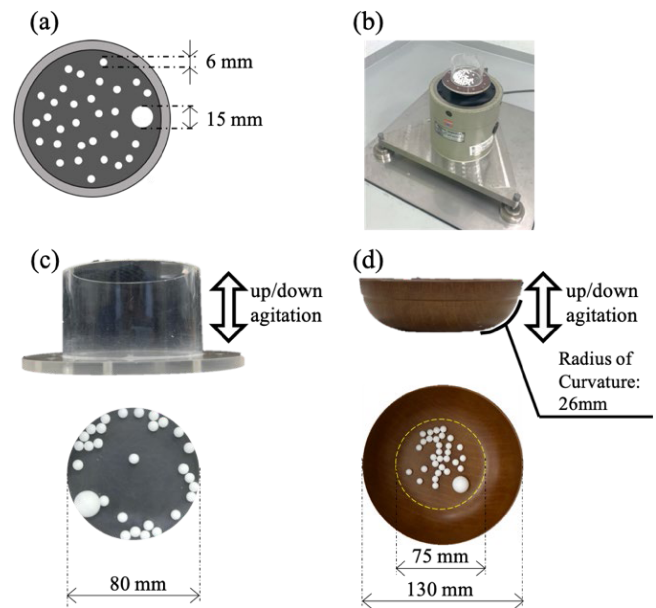

Fig. 1. (Color online) Experimental system to observe the movements of one large and several small particles under vertical vibration. (a) Schematic diagram of the large and small spheres in a container. (b) Electromagnetic shaker used to apply vertical sinusoidal agitation. (c) Side and top views of the cylindrical container, i.e., the hard boundary condition. (d) Side and top views of the round-bottom container, i.e., the soft boundary condition.

of the boundary's hardness/softness, we performed a numerical simulation on a cell-sized micro system under Brownian fluctuation to shed light on the underlying effect boundary conditions may have on living cellular systems.

2. Experimental Macroscopic Modeling of Particles

We investigated the movement of vibrating particles using a model with hard or soft boundaries (Fig. 1). Our experiments were performed with a large particle (15 mm diameter) and many small particles (6 mm diameter) confined in a container under a mechanical up/down vibration. The vertical vibration was applied using an electromagnetic shaker (512 Series Vibration Generator; EMIC Co., Tokyo, Japan), similar to the apparatus arrangement in our previous study.[42] Two different types of containers, cylindrical and bowl-shaped, were adopted for the experiments, and were fabricated at the Yoshimoti Factory Company (Osaka, Japan) under a custom-order from the authors. Their shapes are depicted in Figs. 1(c) and 1(d). Hereafter, these are referred to as "hard" and "soft" confinements, respectively. Sinusoidal agitation in the vertical direction was applied at a frequency of 60 Hz and with an amplitude of 0.21 mm, corresponding to a maximum acceleration of $30 \, \text{m/s}^2$. We tuned the degree of crowding in the container by varying the number of small particles, which influenced the packing fraction, η, to describe the degree of crowding in the system. A packing fraction of $\eta = 1$ corresponded to the condition where small particles were arranged with tight packing over the entire bottom area of the container, with a radius of 80 and 75 mm for the hard and soft boundaries, respectively. We monitored and recorded the dynamics of the larger sphere using a digital CCD camera (EX-100, Casio Computer), with a frame rate of $29.97 \, \text{s}^{-1}$.

Time-dependent changes in the localization of a vibrated large sphere under different degrees of crowding with small

spheres at $\eta = 0.2, 0.4, 0.6, 0.8$ are shown in Fig. 2(a). Experiments were performed using the electromagnetic shaker [Fig. 1(b)] on the cylindrical vessel, i.e., "hard" container [Fig. 1(c)]. The large sphere was always initially placed at the same position at $t = 0$ for these experiments. The trajectories of the center of the large sphere are shown on the right of Fig. 2(a), where the blue and red traces correspond to the time periods of 0–60 and 60–300 s, respectively. It is noted that the red lines correspond to the stationary state. At $\eta = 0.2$, the large sphere occasionally collided with the boundary during the fluctuating motion, whereas it frequently preferred the inner region of the confined space when the degree of crowding was increased. Thus, the location of the large sphere exhibited a transition from the boundary towards the interior with an increase in η. Figure 2(b) shows the radial density of the large sphere, $P(r/r_0)$, evaluated from traces in the stationary state, $t = 60–300$ s, corresponding to the trajectory red lines on the right side of Fig. 2(a). The radial probability clearly demonstrated a drastic change in the position of the large sphere. This change in the probability implies that the localization transition of the large sphere resembles a first-order phase transition.

Figure 3(a) exemplifies the time-dependent changes in the position of a vibrated large sphere together with several smaller spheres, using the round-bottom vessel, i.e., soft container. Time traces are shown on the right, where the blue and red traces correspond to the time periods of 0–60 and 60–300 s, respectively. Figure 3(b) shows the radial density $P(r/r_0)$ for the different degrees of crowding. The large sphere was always initially placed at the same position at $t = 0$ for these experiments and moved from the interior to the boundary with an increase in η. The radial distribution of both large and small particles with the soft boundary condition indicated a similar behavior for particles in Brownian motion under lower degrees of crowding. The radial direction of the large particle tended to distribute around the middle area of a container when the boundary was soft at lower degrees of crowding. The tendency of localization of the large particle in soft boundary is considered that small particles tend to move toward and gather around the center of the cavity due to the interaction by the tilted boundary, which is similar to harmonic interaction, and make a packed confirmation of small particles shown in Fig. 3(a). Thus, the larger particle is localized near the boundary made of crowding small particles at several crowding conditions of $\eta = 0.2, 0.4, 0.6, 0.8$. The boundaries of aggregated small particles at $\eta = 0.2, 0.4, 0.6$ are around $r/r_0 \approx 0.6$.

Thus, spatial localization as a function of the degree of crowding differs between the hard and soft boundaries. The detail explanation of localization of the large particle with small particles in hard and soft boundaries is described in Appendix A.1. We have also observed the large particle in the container with soft/hard boundaries without small particles (see A.2 in Appendix), and found that the single large particle prefers the outer boundary and inner region under the hard and soft boundaries, respectively. Our current vibrating experiments aimed to replicate the entropic effect experienced by confined particles mediated by "hard" and "soft" boundaries, an essential thermodynamic quantity to
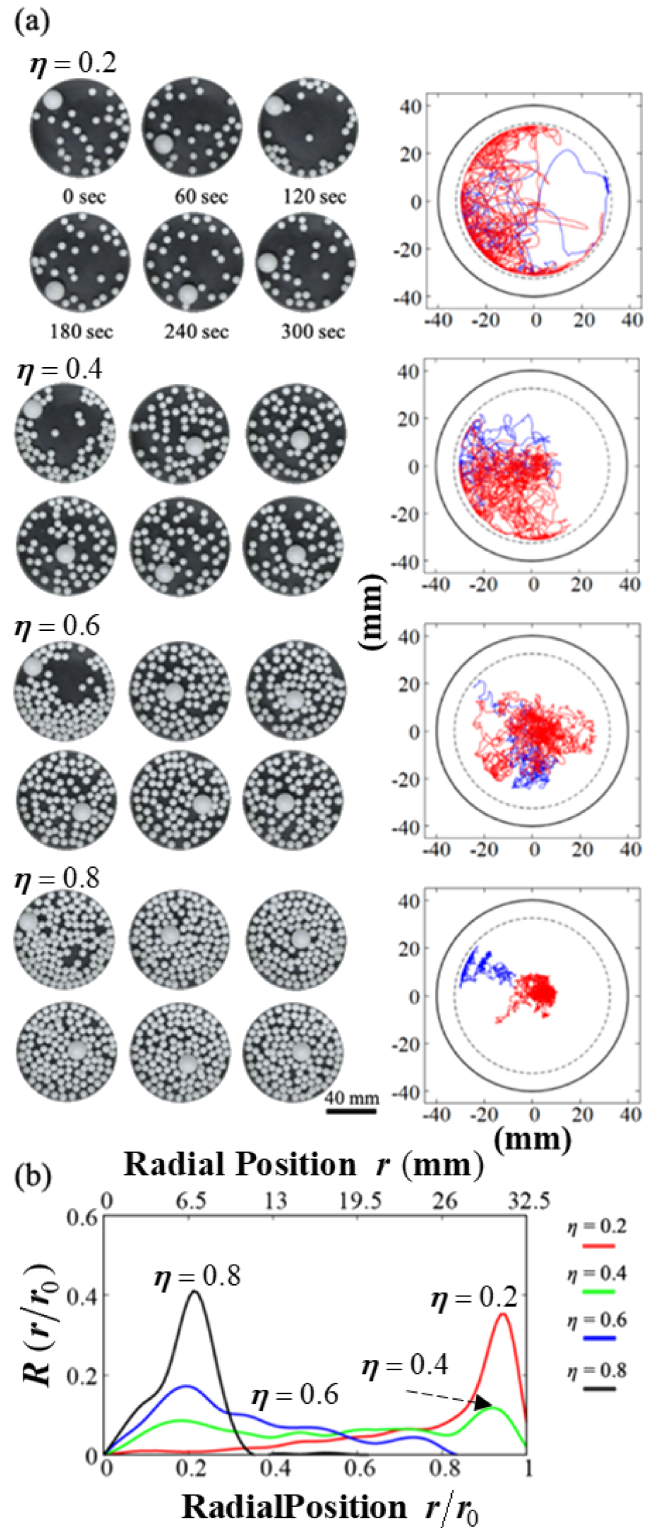

Fig. 2. (Color online) The effect of crowding on a large sphere contained within a hard boundary. (a) Time-dependent changes for the location of the large sphere under different degrees of crowding η with a hard boundary condition. Left, representative snapshots of particles at different times. Right, radial trajectories of the large sphere for the initial ($t = 0$–60 s; blue) and stable ($t = 60$–300 s; red) time periods. The number of small spheres used was $N_s = 28, 56, 84,$ and 112 for $\eta = 0.2, 0.4, 0.6,$ and 0.8, respectively. (b) Radial densities for the large sphere under different degrees of crowding η, corresponding to the red lines shown in (a). The data of the radial positioning are given based on the experiments more than three runs.
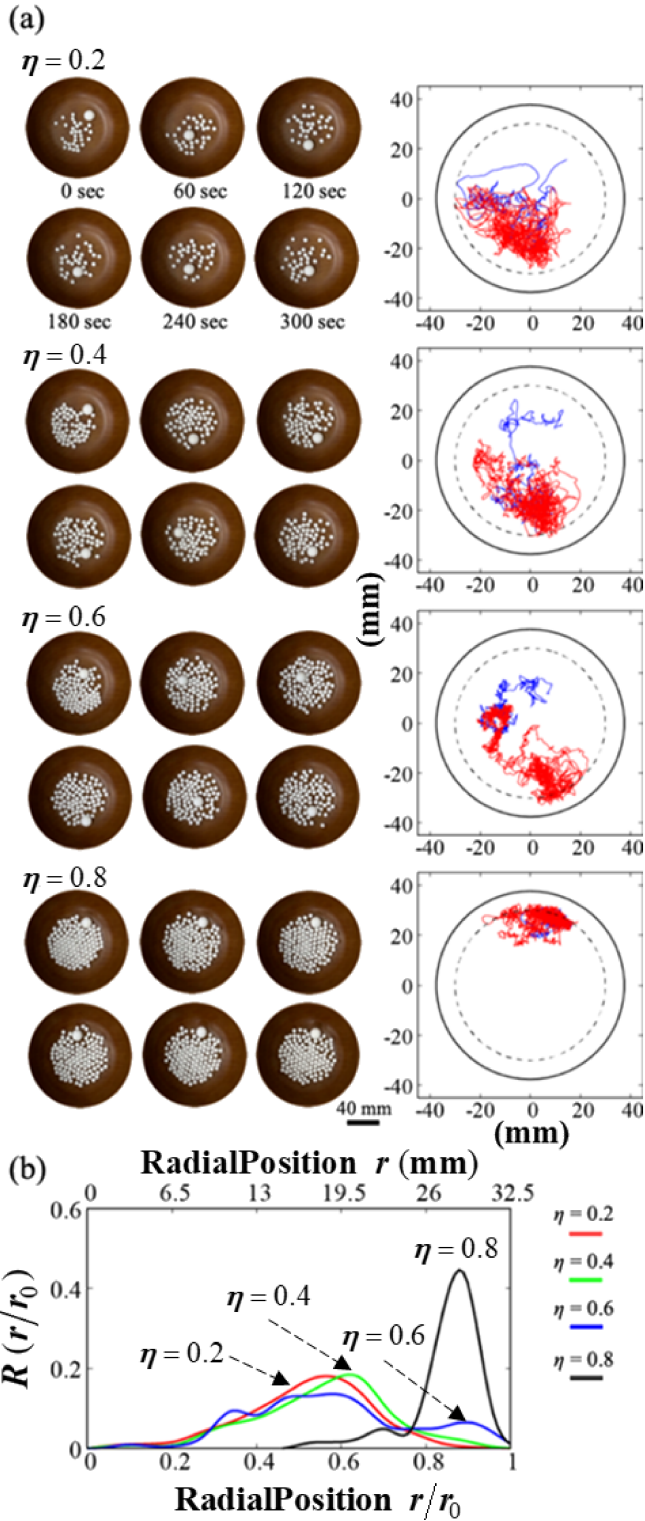
Fig. 3. (Color online) The effect of crowding on a large sphere contained within a soft boundary. (a) Time-dependent changes for the location of the large sphere under different degrees of crowding η with a soft boundary condition. Left, representative snapshots of particles at different times. Right, radial trajectories of the large sphere for the initial ($t = 0$–60 s; blue) and stable ($t = 60$–300 s; red) time periods. The number of small spheres used was $N_s = 30$, 60, 90, and 120 for $\eta = 0.2$, 0.4, 0.6, and 0.8, respectively. (b) Radial densities for the large sphere under different degrees of crowding η, corresponding to the red lines shown in (a). The data of the radial positioning are given based on the experiments more than three runs.

understand a highly crowded living cell. Our finding of the centralization of a larger particle in the inner cavity is consistent with previous experimental and theoretical findings due to the penetration of smaller particles into the area of the larger particle near the boundary.[13,51] The result of the larger particle distributing around the "soft" tilted boundary was previously predicted in the literature based on a three-dimensional model, which attributed the movement to depletion forces imposed on the larger particle by smaller particles near the boundary.[11]

3. Numerical Modeling of Particles as a Cell-Like System

The granular particles in the vibrating plate were under constant agitation against gravity. The frequent collisions among these granular particles led to a scenario resembling particles undergoing random motion in a liquid. The vibrating plate experiment eventually resulted in a steady state like a liquid system with local particle packing due to thermal equilibrium, but in quasi 2D space. To better elucidate the steady states observed in our experiment, we used a Brownian dynamics simulation that consisted of random and dynamical particle motion. Detailed interpretation on the non-deterministic behavior of the particle motion in vibrating plate is given in Appendix A.3 together with Fig. A·3, together with the arguments on the similarity of its stochastic aspect with thermal fluctuation. The hard-sphere-like interactions among granular particles were approximated by simple repulsive forces in the numerical simulation. In our model, we considered one large sphere $N_L = 1$ and multiple smaller spheres N_S to be confined in a cylindrical container. The wall of the cylindrical vibrating plate was oriented either vertically or tilted, as discussed in the experimental section. Each particle was subjected to three types of interactions: (1) each particle is energized by the vibrating plate and undergoes vertical motion; (2) when a particle hits the wall of the vibrating cylinder, it most likely will bounce inward; and (3) particles interact with each other through repulsive forces. To model the oscillating vertical motion, we first assumed that particles were under a harmonic potential along the vertical (or z-) direction as follows:

$$\frac{V(z_i)}{k_B T} = 0.5 k_{z,i}(Z_i - Z_0)^2, \tag{1}$$

where k_B is the Boltzmann constant, T is the temperature, Z_i is the position of the large ($i = 1$) or a small particle ($2 \leq i \leq N_s + 1$), $k_{z,i}$ is the reduced strength of the harmonic potential of a particle I, and $k_{z,i}\sigma^2 = 0.5$ in the simulation. Z_0 is the average height of an isolated particle along the vertical direction, which was the same for both the large and smaller particles and was set at 1.4σ. Note that all distances were measured in terms of a unit length σ. To further simplify the model, the boundary of the vibrating plate was modeled in the following manner. When a particle moved across the boundary horizontally, it triggered a harmonic potential to limit the radial motion of the particle, which is given by

$$\frac{V(z_i)}{k_B T} = 0, \qquad \text{if } r_i \leq R_i$$
$$= 0.5 k_{r,i}(r_i - R_i)^2, \quad \text{if } r_i > R_i \tag{2}$$

Table I. Simulation parameters used for the 2D calculations of Fig. 4.

Cases	Parameters of particle size		Strength of the interaction between particles	
	$\sigma_{1,j}/\sigma$	$\sigma_{i,j}/\sigma$ $(i > 1)$	$\varepsilon_{1,j}$	$\varepsilon_{i,j}$ $(i > 1)$
(a)	0.8	0.5	1.5	1.2
(b)	0.8	0.4	1.2	0.7
(c)	0.8	0.4	1.5	1.2
(d)	0.8	0.4	1.5	1.2

Cases	Harmonic potential of confinement			
	$k_{z,1}\sigma^2$	$k_{z,i}\sigma^2$ $(i > 1)$	$k_{r,1}\sigma^2$	$k_{r,i}\sigma^2$ $(i > 1)$
(a)	1	1	40	40
(b)	1	1	2	6
(c)	1	1	40	40
(d)	1	1	2	6

where r_i is the radial distance from the center of the container to the center of mass of the i-th particle, $k_{r,i}$ is the strength of the repulsive harmonic potential of particle i, and R_i is the boundary for the i-th particle. In the simulation, $k_{r,i}$ and R_i were essential parameters used to adjust the "softness" of the boundary and their values are summarized in Table I. In the vibrating plate experiment, granular particles interacted through rigid-body repulsive forces, which can be viewed as hard-core repulsions in an athermal system. The potentials [Eqs. (2) and (3)] for particle-boundary and inter-particle interactions were chosen for the numerical simulation to represent the repulsive nature of interaction forces, like the work by Awazu.[34] Since the true temperature of granular particles in the vibrating experiment was unknown, the interaction strengths k_{ri} and ε_{ij} in Eqs. (2) and (3) became adjustable parameters relevant to the effective temperature of granular particles. The interaction between particles is given by using the repulsive Lennard-Jones potential as follows:

$$\frac{V(z_i)}{k_{\mathrm{B}}T} = 0, \qquad\qquad\qquad \text{if } r_{ij} \geq r_{c,ij}$$

$$= 24\varepsilon_{ij}\left[\left(\frac{\sigma_{ij}^{12}}{r_{ij}^{12}} - \frac{\sigma_{ij}^6}{r_{ij}^6}\right) - \left(\frac{\sigma_{ij}^{12}}{r_{c,ij}^{12}} - \frac{\sigma_{ij}^6}{r_{c,ij}^6}\right)\right],$$
$$\text{if } r_{ij} \leq r_{c,ij} \qquad (3)$$

where the indexes i and j indicate the i- and j-th particles where $i < j$, r_{ij} is the distance between the i- and j-th particles, σ_{ij} is the sum of the Lennard-Jones radii of the i- and j-th particles, ε_{ij} is the strength of the interaction between the i- and j-th particles, and $r_{c,ij}$ is the cut-off distance that removes the attractive tail in the Lennard-Jones potential between i and j, and is equal to $(2\sigma_{ij})^{\frac{1}{2}}$. We divided all pair interactions into two groups, $(i = 1, j > 1)$ and $(i > 1, j > 1)$, and $i = 1$ was the large sphere because there was only one large sphere. In the simulation, we set $R_1 = 2.17\sigma$ and $R_i = 2.84\sigma$ for $i > 1$. The rest of the parameters are summarized in Table I. Based on the simplified modeling framework described above, we performed a Brownian dynamic simulation in which the i-th particle is initially at $r_i(t)$ and is driven to $r_i(t + \Delta t)$ after a time interval Δt, following the equation given by

$$r_i(t + \Delta t) = r_i(t) + \sum_j D\left(\frac{F_{ij}}{k_{\mathrm{B}}T}\right)\Delta t + \delta r_i^G, \qquad (4)$$

where D is the reduced diffusion constant, Δt is the reduced time interval between two adjacent steps, F_{ij} is the force exerted on the i-th particle by the j-th particle, and δr_i^G is the Gaussian random force of particle i based on Allen and Tildesley;[44] $\langle \delta r_i^G \delta_j^G \rangle = 2D\Delta t$. In the simulation, we choose $D/k_{\mathrm{B}}T = 1$ and $\Delta t = 1 \times 10^{-2}$. For every set of parameters, at least 7.5×10^7 time steps were performed, and the first 2.5×10^7 time steps were discarded for each simulation.

In the vibrating plate experiment, formation of the steady state can be sensitive to several factors, such as effective temperature and energy dissipation processes, due to the non-equilibrium nature of the experiment. A Brownian dynamics simulation was preferable for this work because the balance between temperature and energy dissipation was empirically adjusted by changing the diffusion constant, time step, and interparticle forces. The random fluctuations arising from inelastic collisions and frictions were considered as Gaussian white noise. In the simulation, we monitored the reduced radial density of the large particle $P(r)$ in the x–y plane, where r is the 2D radial distance measured from $x = 0$ and $y = 0$, and $r^2 = x^2 + y^2$ when the large particle is located at the coordinate (x, y). The density distribution function $\rho(r)$ was first calculated from the histogram $H(r)$ when the large particle was between r and $r + \Delta r$, which is given by

$$\rho(r) = \frac{H(r)}{A(r)}, \qquad (5)$$

where $A(r)$ is the area between the interval of the radial distance r and $r + \Delta r$. The reduced density distribution function was then calculated as

$$R(r) = \frac{\rho(r)}{\rho_0(r)}, \qquad (6)$$

where $\rho_0(r)$ $(= 1/\pi r_0^2)$ is the density of a large particle without smaller crowding particles within the circular area of a cavity with a nominal radius r_0 and $r_0 = R_i$ (R_i is defined in the simulation parameters). This reduced density of the distribution function $R(r)$ is analogous to the inverse of the compression factor in real gases. In the simulation, we set $\Delta r = 0.8\sigma$. Note that the nominal packing fraction is defined as $\eta = (r_L^2 + N_s r_s^2)/r_0^2$ where $r_L + r_s = \sigma_{1,j}$ and $2r_s = \sigma_{ij}$. Following the parametrizations given in Table I, we compared the radial density $P(r)$ for different simulation parameters in Figs. 4(a) and 4(b) with different numbers of smaller particles N_s as marked. Note that beyond r_0, $R(r)$ quickly decayed to zero. In Fig. 4(a), $P(r/r_0)$ showed the maximum near $r/r_0 = 0.80$ when $\eta = 0.48$ for $N_s = 32$. As N_s was increased to 44, which corresponded to $\eta = 0.65$, $P(r/r_0)$ became quite flat with roughly 3 weak peaks at $r/r_0 = 0.17, 0.51$, and 0.95. At $\eta = 0.91$ for $N_s = 64$, a peak emerged around $r/r_0 = 0.23$. These results were consistent with our experimental observations with the crowding degrees of 0.2, 0.4, and 0.8 in Fig. 2(b) for the case with a vertical boundary where the large sphere was preferentially located in the interior of the cavity as crowding increased. The effect of crowding on $R(r)$ [Fig. 4(b)] was different from the trend in Fig. 4(a). At a low packing fraction $\eta = 0.34$ with $N_s = 32$, $R(r)$ had a peak emerging near $r/r_0 = 0.27$. For $\eta = 0.48$ with N_s of 48, $R(r)$ was notably flattened. As N_s was increased to 72, $\eta = 0.69$, the peak in $R(r)$ shifted to a higher r (at around $0.96r_0$). These findings were
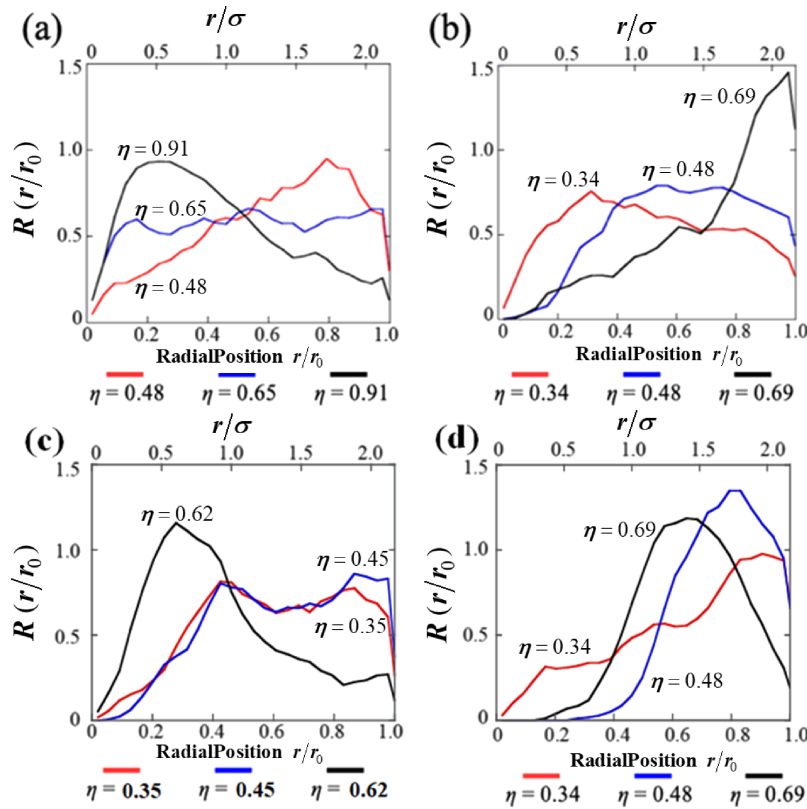
Fig. 4. (Color online) Numerically simulated particle movement determined using a simple 2D model. Radial density of the large sphere for the hard boundary in (a) and (c) and the soft boundary in (b) and (d), respectively. Parameters adopted in the simulation are given in Table I. The number of small spheres used was $N_s = 32$, 44, and 64 for $\eta = 0.48$, 0.65, and 0.91, respectively, in (a) and (c), and $N_s = 32$, 48, and 72 for $\eta = 0.34$, 0.48, and 0.69, respectively, in (b) and (d).

comparable to the behavior observed in the vibrating experiment with a non-vertical boundary (a tilting boundary extended outwards), corresponding to the results for the degrees of crowding of 0.2, 0.6, and 0.8 in Fig. 3(b). In fact, Fig. 4(a) showed how simulated particles mimicked the results for the vibrating plate experiment with a more rigid boundary, whereas simulated particles moved across the boundary more easily when the boundary was softened [Fig. 4(b)].

The major difference between Figs. 2 and 3 was in the boundary of the vibrating plate. In contrast to the vertical wall, the tilted wall introduced "softness" because particles were allowed to move into the space beyond the base of the vibrating plate. In our numerical model, the softer boundary in Fig. 4(b) was achieved by setting the simulation parameter $k_{r,i}$ to be lower than the simulation parameters in Fig. 4(a). In addition to tuning the relative softness of the boundary, to ensure that $R(r)$ behaved like the experimental results, it was essential to change the parameters regarding the extent of vertical motion $k_{z,i}$ and the interacting forces between the large particle and smaller particles (through σ_{ij} and ε_{ij}). These adjustments rendered a phenomenological adaption to model the balance between effective temperature and energy dissipation in the actual experiment.

Consequently, the large particle in a hard boundary was under vertical motion at a higher frequency and showed stronger interactions with smaller particles [Fig. 4(c)]. Under a low degree of crowding, the large particle preferentially distributed near the cavity boundary, which can be explained by the depletion effect. However, under a high degree of

crowding, the ability of the large particle to access the boundary was significantly reduced by the large number of smaller particles, which created a second dynamical wall before the large particle could reach the boundary. Meanwhile, both the boundary and the dynamical wall directed the large particle towards the interior of the cavity.

Reducing both the frequency of the vertical motion of the large particle and the interactions of the large particle with smaller particles gave contrasting results [Fig. 4(b)]. These changes to the simulation parameters increased the chance that the large particle would locate near the boundary. The softer boundary also allowed both types of particles to access the region near the boundary more easily. The combination of these factors was responsible for the observation that the large particle tended to locate closer to the boundary under higher degrees of crowding.

Besides identifying simulation parameters that manifested consistent behaviors with the vibrating plate experiment, we explored the simulation model further in Figs. 4(c) and 4(d). Figure 4(c) had the same parameters as Fig. 4(a) except that $\sigma_{i,j}/\sigma$ was reduced from 0.5 to 0.4. Reduction of σ_{ij}/σ further decreased the size of smaller particles and lowered the packing fraction for each $R(r)$ in Fig. 4(c), even though the number of smaller particles N_s was kept the same as in Fig. 4(a). For the lower packing fractions $\eta = 0.35$ and 0.45, their reduced density distribution functions, $R(r)$, were very close, which showed a bimodal distribution with peaks around $r/r_0 = 0.42$ and 0.9. For the highest packing fraction $\eta = 0.62$, $R(r)$ exhibited a marked peak at $r/r_0 = 0.25$. The results shown in Fig. 4(c) indicate the importance of the

crowding level needed to induce centralization of the large particle in a more rigid boundary. Like Fig. 4(b), the results from a less rigidly bound simulation are shown in Fig. 4(d), but with an increase in the strengths of repulsive interactions among particles. These include $\varepsilon_{i,j}$ (between the larger and any smaller particle) and $\varepsilon_{i,j}$ $(i, j > 1)$ (between any two smaller particles) (Table I), by keeping the same packing fractions in the two plots. For the case of the lowest packing fraction, $\eta = 0.34$, in Fig. 4(d), $R(r)$ showed a peak near the boundary, $r = 0.9r_0$. This result suggests that the strong repulsive interactions among particles induced a stronger depletion force on the larger particle so that it was pinned near the boundary. The peaks shifted towards the inner cavity around $r/r_0 = 0.8$ and 0.6 for $\eta = 0.48$ and 0.69, respectively, as the packing fraction increased. This trend indicates that the smaller particles tended to distribute around the boundary to alleviate repulsions among smaller particles. As a result, the larger particle moved towards the inner cavity to further accommodate more repulsive smaller particles around the boundary. The predictions arising from the results shown in Figs. 4(c) and 4(d) can be tested in future experiments by changing the size ratio between the large and small granular particles and by changing the design of the soft boundary on the vibrating plate.

These finding are consistent with our previous work using a Monte Carlo simulation,[45] which showed that the large particle was centralized or depleted from the central region of the confined cavity, depending on the conditions. The mechanism that underlies these trends involves a thermodynamic pathway more than a dynamic pathway. Although the vibrating plate experiment was conducted under conditions very different from those for the simulation, the experimental trends for specific positioning under crowing conditions were comparable to the numerical results obtained using Brownian dynamics simulations for a confined system under crowding. Particles inside the cavities collide with each other stochastically under a mechanical up/down vibration, which generates the stochasticity of particle motions in the athermal system. Stochasticity of the motion in the athermal system causes a similar tendency on the stochastic motion of Brownian dynamics in thermal system based on the experimental and simulation results.

4. Conclusion

We studied the localization behavior of a large particle in the presence of several small particles confined in containers with hard or soft boundary conditions under mechanical vibration. The experimental results indicated that the degree of crowding by small spheres governed the localization of the large sphere with respect to the boundary. The large sphere was located near the boundary of the container when there was a low degree of crowding ($\eta = 0.2$) and near the interior of the container for a high degree of crowding ($\eta = 0.8$) with a hard boundary condition in a self-organized manner. The location of the large sphere showed an opposite trend in the container with a soft boundary. Simulation results based on Brownian dynamics duplicated the experimental findings regarding the location of the large sphere. The degree of crowding and the boundary condition directly contributed to where the large sphere localized based on the experimental and calculated results. Importantly, this work elucidated

physical insights into our vibrating plate experiment. The numerical model chosen in this study mimicked randomly fluctuating motion and local packing of granular particles in the vibrating plate experiment. We applied simplified repulsive forces to approximate the hard-sphere like interactions among granular particles. We found the steady states evolved in the vibrating experiment could be qualitatively interpreted by using this simple liquid state model. Namely, via a careful design, the vibrating plate may become a macroscopic tool to study thermal fluctuating microscopic systems. Studies of stochastic fluctuation in nature at the microscopic scale are essential to understand the spatial length and time scales required for a macroscopic system to arrive at a steady or an equilibrium state with a deterministic nature, such as a living cell. We expect that our experimental findings will help to describe the self-organization of the nucleus in a cell, which is in a space crowded by biopolymers within a membrane. The present results suggest that the stiffness of the cell membrane may play an essential role in the dynamics of biopolymers including the nucleus, which can control cell function. We also expect that our findings provide a fundamental understanding of membrane stiffness and will be key to revealing different effects between animal and plant cells, as a next extension of the present study.

Appendix

A.1   Behavior of a large particle with hard/soft boundaries

These results and the relevant work in literature[10–13,51] together provide a possible physical picture to the distinctly different behavior between a hard and a soft boundary as shown in the schematic explanation of Fig. A·1. While a particle distributes next to a hard boundary, the surrounding particles induce depletion forces and tend to localize the particle next to the boundary. The size disparity of the large and small particle allows small particles to distribute under the large sphere [left panel in Fig. A·1(a)]. This "penetration" process weakens the depletion force experienced by the large particle[51] and it is pushed away from the boundary due to frequent collisions from small particles arising from the side close to the boundary and underneath of the large sphere [middle panel in Fig. A·1(a)]. As such, the large particle desorbs from the boundary. Once the large particle shifts away from the boundary, it undergoes more collisions from the small particles distributed at a longer radial distance than those at a shorter radial distance [right panel in Fig. A·1(a)] because the number of small particles increases from the cavity center to the boundary. The large particle is expected to move toward the center of the cavity where the net force exerted on the large particle is essentially zero. Whereas, under a soft boundary, the small particles collide with the large particle and trap it on the titled boundary [Fig. A·1(b)].

A.2   Behavior of a single large particle in the container with soft/hard boundaries without small particles

Figure A·2 shows time-dependent changes in the localization of a vibrated large sphere without small particles. The
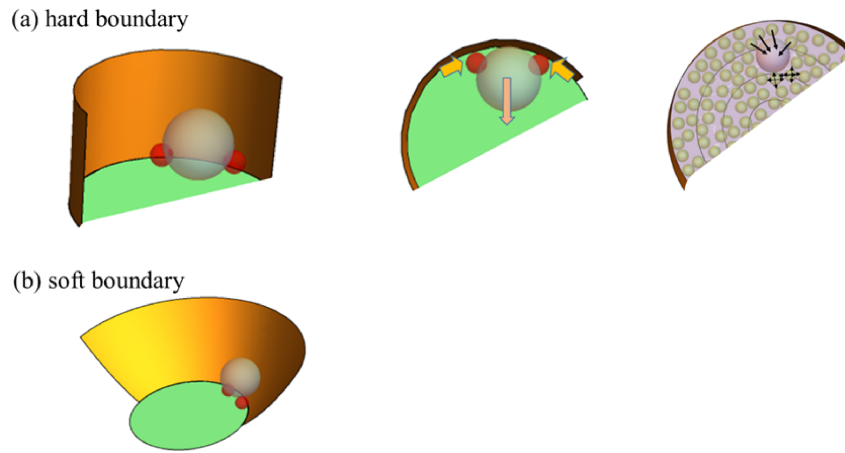
Fig. A·1. (Color online) Localization of the large particle. (a) Left panel: Small particles penetrate the large particle from the bottom due to size disparities. Middle panel: Small particles induce depletion forces on the large particle and it desorbs from the boundary. Right panel: Small particles closer to boundary have more anisotropic collisions on the large particle than those in inner cavity under multiple collisions from surrounding small particles. (b) Small particles can lift the large particle on the tilted boundary and trap it near the boundary in higher degree of the crowding.
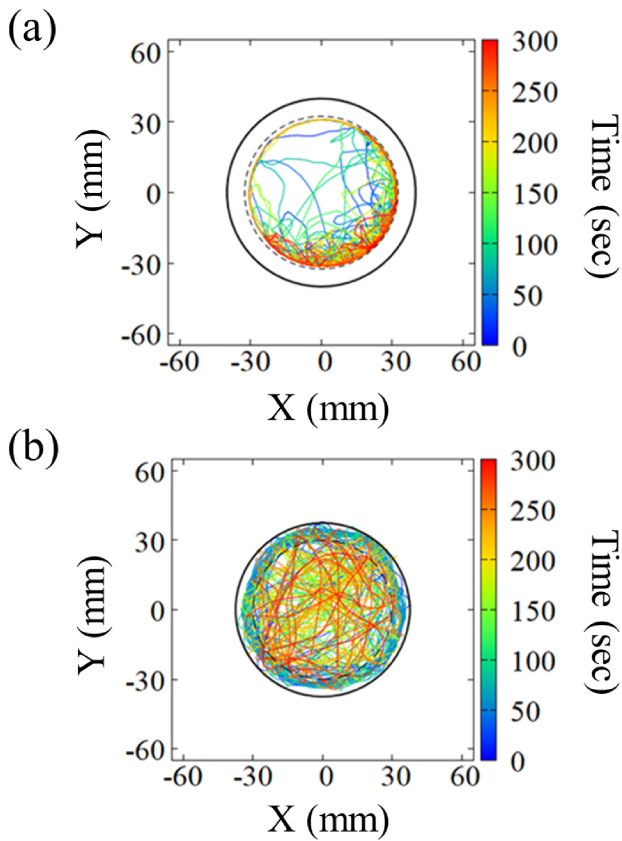

Fig. A·3. (Color online) Time-dependent vertical position of a single large (or small) particle with a frequency of 60 Hz and maximum acceleration of $30 \, \text{m/s}^2$.

Fig. A·2. (Color online) Time-dependent changes for the location of the large sphere (a) Radial trajectories of the large sphere with a hard boundary condition. (b) Radial trajectories of the large sphere with a soft boundary condition.

A.3 Time-dependent vertical position of a single large and small particle on the vibrating plate

An additional experiment was carried out to study the motion of a single large particle and of a single small particle, respectively, on a vibrating plate by analyzing the time-dependent vertical position of each particle as shown in Fig. A·3. We find that their vertical positions display a random pattern, like noises. Such noises may originate from the following facts. The observed vertical height of a particle depends on the duration between the moment that the particle landed on the plate and the time it experienced the upward force again. In other words, after the particle landed on the plate, the amount of energy dissipation of the particle onto the vibrating plate may dictate its next vertical position. As a result, we observe non-deterministic behavior of the motion of a single particle. In the real experiment, there are more particles placed in the vibrating plate along with the boundary wall of the container, which complicate the energy dissipation processes of particles and noise propagations among particles further. To account for the experimental observation, it is instructive to apply a numerical simulation model that has the component of noises. Note that the noises are to account for the non-deterministic behavior of particle motion observed in Fig. A·3 in a qualitative fashion.

experimental result indicated that the particle tends to distribute almost uniformly inside the cavity with soft boundary. Meanwhile, the particle is localized near the wall of the cavity in the hard boundary condition. Notice that these results serve as a control to indicate the crowding effect of small particles on the localization of the large particle, comparing with the distribution of the test particle in the crowding conditions with small particles shown in Figs. 2 and 3.
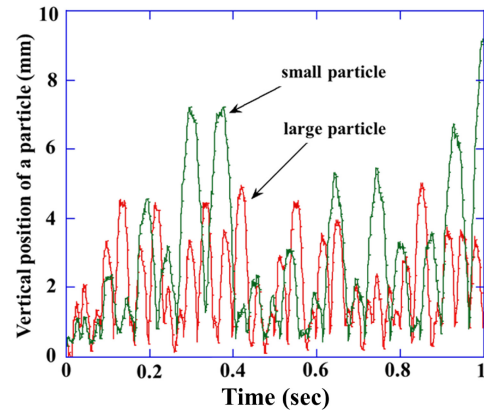
*amymtkhy.8o.ran@gmail.com
†fiddich.2006-12.20@outlook.com
‡Corresponding author. E-mail: tkenmots@mail.doshisha.ac.jp
§keyoshik@mail.doshisha.ac.jp
¶Corresponding author. E-mail: chwenyang.shew@csi.cuny.edu

1) S. B. Zimmerman and S. O. Trach, J. Mol. Biol. **222**, 599 (1991).
2) R. J. Ellis, Curr. Opin. Struct. Biol. **11**, 114 (2001).
3) H. X. Zhou, G. Rivas, and A. P. Minton, Annu. Rev. Biophys. **37**, 375 (2008).
4) I. M. Kuznetsova, K. K. Turoverov, and V. N. Uversky, Int. J. Mol. Sci. **15**, 23090 (2014).
5) S. Asakura and F. Oosawa, J. Chem. Phys. **22**, 1255 (1954).
6) S. Asakura and F. Oosawa, J. Polym. Sci. **33**, 183 (1958).
7) Y. Mao, M. E. Cates, and H. N. Lekkerkerker, Physica A **222**, 10 (1995).
8) H. N. Lekkerkerker and R. Tuinier, *Colloids and the Depletion Interaction* (Springer, Berlin, 2011) Lecture Notes in Physics, Vol. 833, Chap. 2, p. 57.
9) K. Miyazaki, K. S. Schweizer, D. Thirumalai, R. Tuinier, and E. Zaccarelli, J. Chem. Phys. **156**, 080401 (2022).
10) C. Y. Shew and K. Yoshikawa, Chem. Phys. Lett. **590**, 196 (2013).
11) C. Y. Shew, K. Kondo, and K. Yoshikawa, J. Chem. Phys. **140**, 024907 (2014).
12) C. Y. Shew and K. Yoshikawa, J. Phys.: Condens. Matter **27**, 064118 (2015).
13) S. Oda, K. Kubo, C. Y. Shew, and K. Yoshikawa, Physica D **336**, 39 (2016).
14) C. Bechinger, R. Di Leonardo, H. Löwen, C. Reichhardt, and G. Volpe, Rev. Mod. Phys. **88**, 045006 (2016).
15) A. A. Glagoleva, V. V. Vasilevskaya, K. Yoshikawa, and A. R. Khokhlov, J. Chem. Phys. **139**, 244901 (2013).
16) M. Tabaka, T. Kalwarczyk, J. Szymanski, S. Hou, and R. Holyst, Front. Phys. **2**, 54 (2014).
17) T. Yamamoto and H. Schiessel, Langmuir **32**, 3036 (2016).
18) S. Jahanshahi, H. Löwen, and B. Ten Hagen, Phys. Rev. E **95**, 022606 (2017).
19) S. Kohyama, N. Yoshinaga, M. Yanagisawa, K. Fujiwara, and N. Doi, eLife **8**, e44591 (2019).
20) L. L. Gutierrez-Martinez and M. Sandoval, J. Chem. Phys. **153**, 044906 (2020).
21) A. Moncho-Jordá and J. Dzubiella, Phys. Rev. Lett. **125**, 078001 (2020).
22) G. Chauhan, M. L. Simpson, and S. M. Abel, J. Chem. Phys. **155**, 034904 (2021).
23) A. Awazu, Phys. Rev. E **90**, 042308 (2014).
24) A. Awazu, Phys. Rev. E **92**, 032709 (2015).
25) P. R. Cook and D. Marenduzzo, J. Cell Biol. **186**, 825 (2009).
26) G. Juarez, I. C. Christov, J. M. Ottino, and R. M. Lueptow, Chem. Eng. Sci. **73**, 195 (2012).
27) C. Jeon, Y. Jung, and B. Y. Ha, Soft Matter **12**, 9436 (2016).
28) A. Zinchenko, Adv. Colloid Interface Sci. **232**, 70 (2016).
29) C. Watanabe and M. Yanagisawa, Phys. Chem. Chem. Phys. **20**, 8842 (2018).
30) A. Deblais, T. Barois, T. Guerin, P. H. Delville, R. Vaudaine, J. S. Lintuvuori, J. F. Boudet, J. C. Baret, and H. Kellay, Phys. Rev. Lett. **120**, 188002 (2018).
31) A. Opathalage, M. M. Norton, M. P. Juniper, B. Langeslay, S. A. Aghvami, S. Fraden, and Z. Dogic, Proc. Natl. Acad. Sci. U.S.A. **116**, 4788 (2019).
32) F. Wu, P. Swain, L. Kuijpers, X. Zheng, K. Felter, M. Guurink, J. Solari, S. Jun, T. S. Shimizu, D. Chaudhuri, B. Mulder, and C. Dekker, Curr. Biol. **29**, 2131 (2019).
33) M. L. Ross, J. Kunkel, S. Long, and S. P. Asuri, Int. J. Mol. Sci. **21**, 8516 (2020).
34) D. Garenne, A. Libchaber, and V. Noireaux, Proc. Natl. Acad. Sci. U.S.A. **117**, 1902 (2020).
35) V. Poulichet, M. Morel, S. Rudiuk, and D. Baigl, J. Colloid Interface Sci. **573**, 370 (2020).
36) J. Steinkühler, E. Sezgin, I. Urbančič, C. Eggeling, and R. Dimova, Commun. Biol. **2**, 337 (2019).
37) M. Bottone, G. Santin, F. Aredia, and G. Bernocchi, Cells **2**, 294 (2013).
38) S. Elmore, Toxicol. Pathol. **35**, 495 (2007).
39) Y. Zhang, X. Chen, C. Gueydan, and J. Han, Cell Res. **28**, 9 (2018).
40) S. Braig, B. S. Schmidt, K. Stoiber, C. Händel, T. Möhn, O. Werz, R. Müller, S. Zahler, A. Koeberle, J. A. Käs, and A. M. Vollmar, New J. Phys. **17**, 083007 (2015).
41) J. G. Downs, N. D. Smith, K. K. Mandadapu, J. P. Garrahan, and M. I. Smith, Phys. Rev. Lett. **127**, 268002 (2021).
42) P. W. Fowler, J. Hélie, A. Duncan, M. Chavent, H. Koldsø, and M. S. Sansom, Soft Matter **12**, 7792 (2016).
43) J. S. Olafsen and J. S. Urbach, Phys. Rev. Lett. **81**, 4369 (1998).
44) P. M. Reis, R. A. Ingale, and M. D. Shattuck, Phys. Rev. Lett. **96**, 258001 (2006).
45) A. Kudrolli, G. Lumay, D. Volfson, and L. S. Tsimring, Phys. Rev. Lett. **100**, 058001 (2008).
46) Y. Komatsu and H. Tanaka, Phys. Rev. X **5**, 031025 (2015).
47) X. Sun, Y. Li, Y. Ma, and Z. Zhang, Sci. Rep. **6**, 24056 (2016).
48) S. Takatori, H. Baba, T. Ichino, C.-Y. Shew, and K. Yoshikawa, Sci. Rep. **8**, 437 (2018).
49) J. Downs, N. D. Smith, K. K. Mandadapu, J. P. Garrahan, and M. I. Smith, Phys. Rev. Lett. **127**, 268002 (2021).
50) M. P. Allen and D. J. Tildesley, *Computer Simulation of Liquids* (Clarendon, Oxford, U.K., 1987) 2nd ed., Chap. 2, p. 46.
51) C. Y. Shew, S. Oda, and K. Yoshikawa, J. Chem. Phys. **147**, 204901 (2017).